Device

Article

An implantable system for opioid safety

Graphical abstract

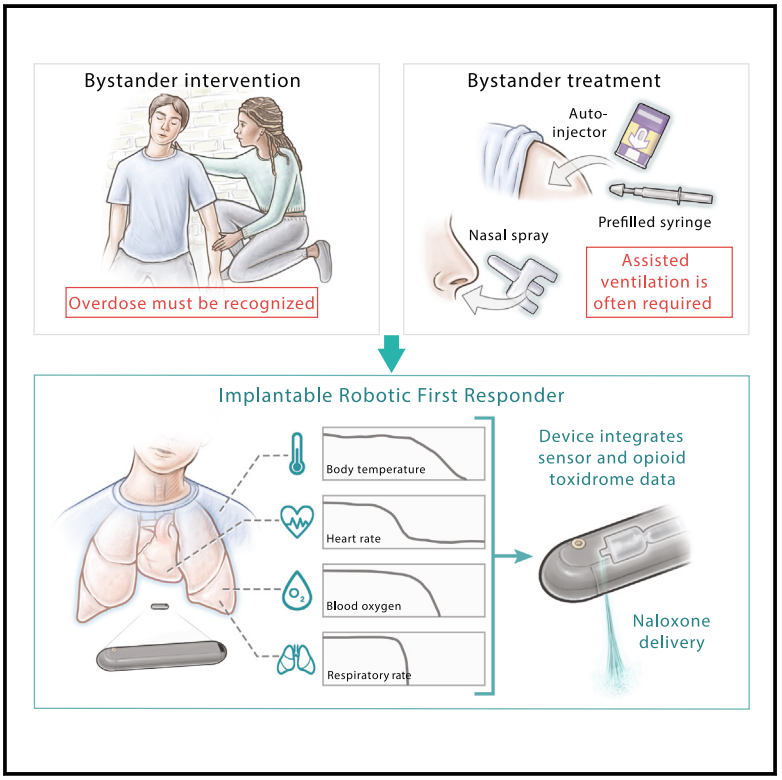

Highlights

- An implantable system that detects opioid overdose and automatically delivers naloxone
- A sensor fusion algorithm accurately detects opioid overdose
- iSOS could help protect patients from fatal opioid overdose
- iSOS evaluation in a swine opiate overdose model

Authors

Hen-Wei Huang, Peter R. Chai, Seungho Lee, ..., Alison M. Hayward, Anantha Chandrakasan, Giovanni Traverso

Correspondence

cgt20@mit.edu

In brief

The implantable SOS (iSOS) consists of a suite of sensors that measure vital signs combined with a drug reservoir that stores naloxone. When the iSOS detects a combination of vital signs indicating an opioid overdose, naloxone is released from the reservoir, which helps reverse the overdose. This study describes the device's development, validation, and preliminary studies in a pig model.

4 Validate
Functional device with real-world testing, ready to scale

Huang et al., 2024, Device 2, 100517
October 18, 2024 Published by Elsevier Inc.
https://doi.org/10.1016/j.device.2024.100517

CellPress

Device

CellPress
OPEN ACCESS

Article

An implantable system for opioid safety

Hen-Wei Huang,[1,2,3,10] Peter R. Chai,[2,4,5,6,10] Seungho Lee,[1,2,10] Tom Kerssemakers,[1,10] Ali Imani,[1,10] Jack Chen,[1,2,3,10] Marco Heim,[1] Jessica Y. Bo,[1] Adam Wentworth,[1,2,3] Fokion T. Sanoudos-Dramaliotis,[1] Ian Ballinger,[1,3] Saurav Maji,[7] Matt Murphy,[3] Alexander Alexiev,[1] Gloria H. Kang,[2] Niora Fabian,[2,3,8] Josh Jenkins,[3] Andrew Pettinari,[2] Keiko Ishida,[2] Jason Li,[1,2,9] Siheng Sean You,[1,2] Alison M. Hayward,[2,3,8] Anantha Chandrakasan,[7] and Giovanni Traverso[1,2,3,9,11,*]

[1]Division of Gastroenterology, Department of Medicine, Brigham and Women's Hospital, Harvard Medical School, Cambridge, MA 02139, USA

[2]Koch Institute for Integrated Cancer Research, Massachusetts Institute of Technology, Cambridge, MA 02139, USA

[3]Department of Mechanical Engineering, Massachusetts Institute of Technology, Cambridge, MA 02139, USA

[4]Department of Emergency Medicine, Brigham and Women's Hospital, Harvard Medical School, Boston, MA 02115, USA

[5]Department of Psychosocial Oncology and Palliative Care, Dana Farber Cancer Institute, 75 Francis St., Boston, MA 02115, USA

[6]The Fenway Institute, 1340 Boylston St., Boston, MA 02215, USA

[7]Department of Electrical Engineering and Computer Science, Massachusetts Institute of Technology, Cambridge, MA, USA

[8]Division of Comparative Medicine, Massachusetts Institute of Technology, Cambridge, MA 02139, USA

[9]Broad Institute of MIT and Harvard, Cambridge, MA 02139, USA

[10]These authors contributed equally

[11]Lead contact

*Correspondence: cgt20@mit.edu

https://doi.org/10.1016/j.device.2024.100517

THE BIGGER PICTURE The opioid epidemic continues to cause significant morbidity and mortality across the US. The implantable system for opioid safety (iSOS) is an implantable, autonomous device that measures vital signs and detects opioid overdose events. The system is implanted under the subcutaneous tissue, has a rechargeable battery that can last up to 14 days, and contains an integrated, refillable drug reservoir that holds a 10-mg naloxone payload. Detection of opioid overdose is facilitated by a unique sensor-fusion algorithm that confirms a likely opioid overdose. A pumping mechanism then rapidly infuses naloxone to reverse the overdose. Testing of the components of the iSOS in a swine model demonstrates the ability of the iSOS to detect both rapid opioid overdose with apnea and gradual opioid poisoning with hypopnea, for both of which naloxone is indicated. The iSOS is a system that may ultimately benefit patients and clinical providers by providing individuals with opioid use disorder with an extra layer of protection to prevent a fatal overdose.

SUMMARY

Naloxone can effectively rescue victims from opioid overdose, but less than 5% survive due to delayed or absent first responder intervention. Current overdose reversal systems face key limitations, including low user adherence, false positive detection, and slow antidote delivery. Here, we describe a subcutaneously implanted robotic first responder to overcome these challenges. This implantable system for opioid safety continuously monitors vital signs, detecting opioid overdose through an algorithm analyzing the interplay of cardiorespiratory responses. To address battery concerns with continuous monitoring and multi-sensing modality, an adaptive algorithm dynamically adjusts sensor resolution, reducing the need for frequent charging. Furthermore, the implant includes an ultra-rapid naloxone delivery pump, delivering the 10-mg antidote within 10 s. In animal trials, the robotic first responder successfully revived 96% of overdosed pigs (n = 25) within 3.2 min, showcasing its potential to dramatically improve survival rates and combat the opioid epidemic.

INTRODUCTION

The opioid epidemic continues to have devastating effects in the US, leading to high rates of morbidity and mortality. Overdose poses a significant risk for individuals using both pharmaceutical and illicit opioids, often resulting in death or the development of opioid use disorder (OUD).[1,2] To combat this crisis, strategies such as informed prescribing, the use of medications for OUD (MOUDs), like buprenorphine and methadone, and harm reduction through naloxone administration have been implemented.[3,4]

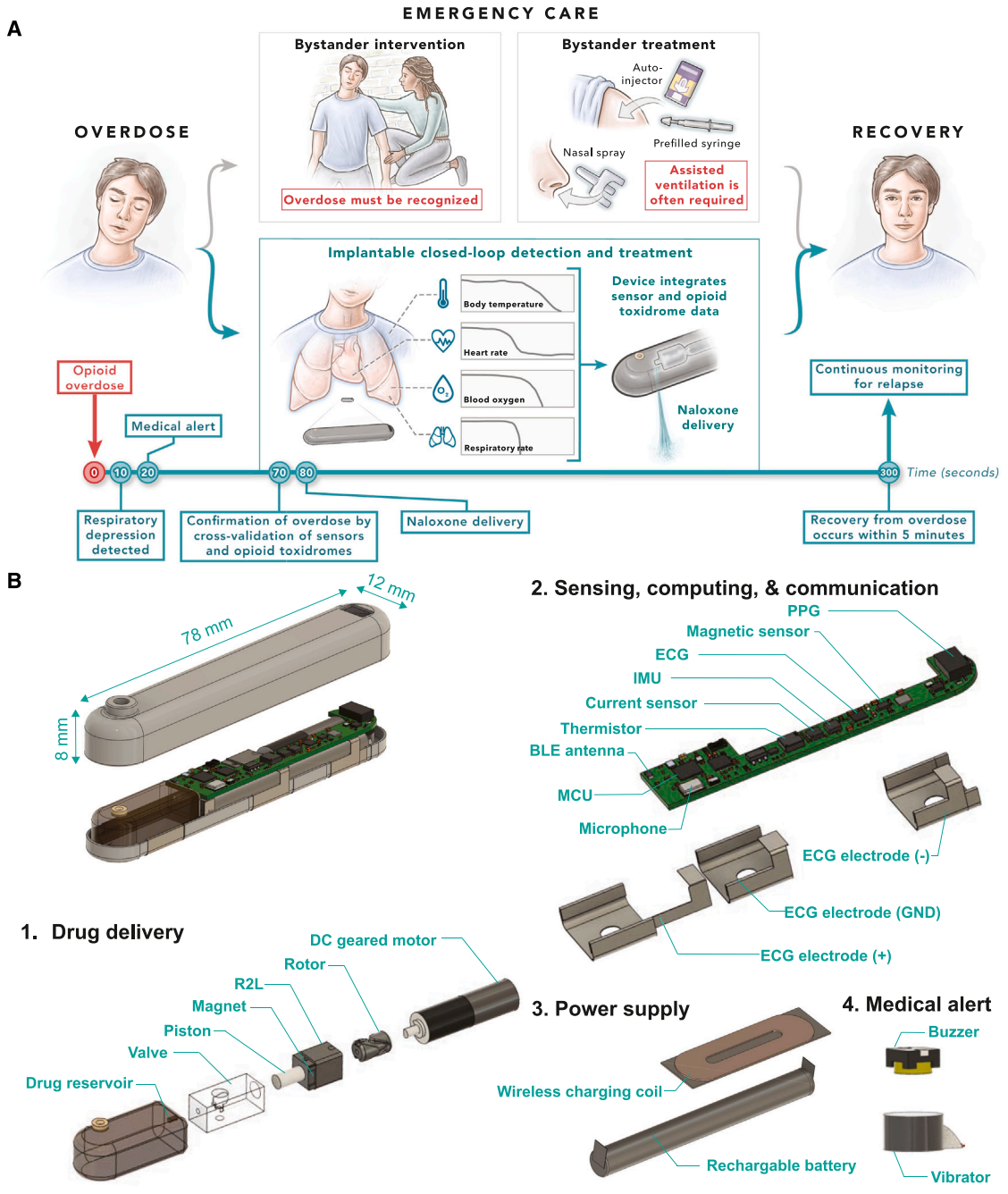

(legend on next page)

The increasing presence of fentanyl in illicit opioids is now contributing to a new wave of opioid-related overdose deaths. Excessive agonism of the μ-opioid receptor, whether from illicit opioid use or inadvertent use of opioids, results in opioid toxidrome, consisting of miosis, respiratory depression (RD), and central nervous system depression. Death occurs through the deleterious effects of RD and respiratory arrest (RA). In the setting of the modern ultrapotent and illicit fentanyl era, loss of consciousness may occur during opioid use, preventing individuals from administering antidotal therapy or providing respiratory support.[3,4] Cerebral injury can become permanent as early as 3 min after the onset of RA, potentially leading to death within 4–6 min.[5,6] While harm reduction strategies coach individuals who seek to use opioids to be in the presence of others to help prevent overdose mortality, provide safe injection sites, or deploy test strips to help individuals recognize the risk of overdose, these strategies are suboptimal in delivering an antidote to individuals who experience opioid overdose.[7,8] Many of these harm reduction strategies were significantly reduced during the COVID-19 pandemic as public health measures encouraged social distancing.[9,10] As a result, opioid overdose death has dramatically increased during the pandemic, reaching a record high of 100,000 in the US in 2021 and continues to be a problem of high public health significance.[11] Consequently, there is an urgent need for technological advancements that provide opioid users with an unobtrusive system that accurately detects overdose and facilitates rapid automated naloxone administration and assistance to ensure full recovery after antidote administration without causing brain injury.

To date, multiple strategies have been developed to better detect and respond to opioid overdose events. Because individuals may develop waxing and waning tolerance to opioids depending on use patterns, periods of sobriety, or treatment with MOUDs, wearable and semi-implantable devices focus on detecting reliable changes in physiology (decreased respiratory rate, RA, or hypoxia) to indicate the onset of opioid overdose. Closed-loop systems then seek to call first responders or close contacts or even administer rescue doses of naloxone.[12–16] Unfortunately, these technologies are currently facing various challenges, including poor patient adherence to continuous monitoring, false-positive detection, slow naloxone administration, and engineering to develop acceptable devices.[17–19] Patients' compliance with wearable electronics is often compromised when sensors are removed, leading to interruptions in continuous monitoring.[20–22] Additionally, poor optimization of power consumption results in the need for frequent battery recharging, which also affects compliance with these technologies. Furthermore, the complex dynamics of cardiorespiratory coupling and limited sensor modalities easily result in false-positive or delayed detection of overdose. Thus far, existing decision-making algorithms for delivering naloxone tend to rely on the detection of apnea or hypoxia, which can lead to poor signal capturing, emulated through intentional breath holding or other medical conditions such as sleep apnea, making consistent overdose detection unreliable.[13,14,16,23] False-positive sensing and incorrect administration of an antidote are important reasons that decrease the willingness of individuals with OUD to engage with such technologies.[17,24,25]

While some of these wearable systems also administer naloxone in the setting of a detected overdose, the real-world applicability and pharmacokinetics of drug administration are suboptimal. For example, proposed devices may administer naloxone too slowly to effectively reverse opioid overdose or may carry a dose of naloxone that is insufficient to counter the opioid effects of nonpharmaceutical fentanyl, which is increasingly prevalent in the illicit opioid supply.[26–28] Additionally, because the onset and severity of overdose is much more rapid in the setting of fentanyl, naloxone must be administered effectively as soon as overdose is detected. Current autonomous systems experience delays not only in the slow release of the antidote but also in the overdose detection and subsequent decision-making for naloxone delivery due to the lack of understanding of the transient response of the interplay of cardiorespiratory signals.[12,13,23]

In response to the existing challenges in autonomous detection of opioid overdose and administration of reversal treatment, we introduce the implantable system for opioid safety (iSOS): a subcutaneously (s.c.) implantable robotic first responder (Figure 1A). This system combines multiple sensor modalities to enable real-time and precise overdose detection, integrates a medical alert system featuring auditory and tactile signals, and incorporates an ultra-fast naloxone delivery module within a compact unit. The system achieves real-time overdose detection by continuously monitoring cardiorespiratory signals and identifying unique physiological biomarkers indicative of an overdose event. When a suspected overdose is detected, the system activates an alarm through auditory and tactile cues while simultaneously sending an alert to the user's smartphone. This alert allows users to override the decision for naloxone administration in case of a false-positive detection. The primary objective behind developing this robotic first responder is to provide a system that autonomously supports individuals who experience opioid overdose, records these events for ongoing OUD care, and reduces the mortality from the opioid epidemic.

RESULTS

The iSOS introduces a compact form factor, measuring 8 × 12 × 78 mm, similar to that of an implantable loop recorder.[29] Our inspiration for selecting a fully implantable system centers around mitigating potential noncompliance with a wearable device and providing effective naloxone reversal in the moment

Figure 1. The s.c. robotic implant designed for continuous monitoring of diverse vital signs and rapid administration of therapeutic agents in emergency care scenarios

(A) Schematics illustrating a human-based and robotic first responder in rescuing victims from overdose.

(B) An exploded CAD model showcasing the implantable system, including various sensors, a drug delivery compartment, and circuits for power supply and onboard computation.

(C) Optical images depicting (i) the robotic implant, (ii) its placement in the trocar, (iii) *in vivo* implantation via the trocar, and (iv) the device post implementation.

overdose occurs. By developing a form factor and implantation process that mirrors a loop recorder, our device has the potential to minimize nonadherence, reliably record physiologic changes associated with opioid overdose, and facilitate effective naloxone administration. We also selected the implantation site to be in the s.c. space to minimize mechanical irritation during implantation. We recognize that externalization of sensors to facilitate a semi-implantable system would reduce the size of the implant, but this strategy risks both noncompliance with the externalized components of such a system and the potential for interference with adequate data collection. While an implantable device with a full sensor suite is larger, the significant advantage of facilitating data collection and seamless closed-loop decision-making advances potential options for patients who may most need support against opioid overdose during the course of their recovery. As shown in Figures 1B and S1, the implantable system is composed of four compartments. The first compartment is designed for rapid naloxone delivery and mainly consists of a drug reservoir, an actuator incorporated with two check valves and a rotational-to-linear (R2L) converter, and a direct current (DC)-brushed geared motor. Moreover, to monitor the motor movement, we embedded a linear magnetic encoder composed of two hall-effect sensors and a magnet in the R2L converter. The iSOS has a flexible drug reservoir made of polyurethane and a port to allow for percutaneous drug refilling. The second compartment houses the multi-sensor array responsible for monitoring various vital signs, microcontroller unit (MCU) for conducting onboard computations, and Bluetooth module for enabling remote updates of the iSOS. The multi-sensor array incorporates an electrocardiography (ECG), photoplethysmography (PPG), thermometer, and inertial moment unit (IMU), which together capture respiratory rate (RR), heart rate (HR), HR variability (HRV), body temperature, and blood oxygen saturation (SpO_2). Figure S1 also shows the algorithms for onboard computation of the vital signs captured by ECG, PPG, and IMU. The onboard computation capacity eliminates the need for additional devices, like a wearable receiver or a smartphone, and enables the iSOS to make therapeutic decisions independently. Physiologic data are captured using the concept of sensor redundancy, which allows for real-time cross-validation of various respiratory and cardiovascular signals, thereby minimizing the occurrence of false-positive detection. The third compartment is dedicated to wireless charging and onboard power supply, allowing operation over sustained periods of time. The last compartment is the medical alert system, composed of a buzzer and vibrational system that is triggered to wake up the user after the detection of an overdose, through which the user can terminate the naloxone delivery when there is a false-positive detection. Implantation of the system is facilitated by a custom trocar, inspired by loop recorders, as depicted in Figures 1C and S2. This trocar facilitates a minimally invasive procedure that can be completed under local anesthesia, requiring only a small incision of 15 mm.

Transient dynamic response of fentanyl overdose

It has been demonstrated that the administration of fentanyl can lead to acute RD and induce both acute and chronic cardiovascular complications in individuals. These complications include bradycardia, hypoxia, and hypotension. While these effects are well documented in clinical settings, there remains a lack of understanding regarding their transient dynamic responses, especially in the critical minutes following an overdose. One notable challenge is the considerable variation in how individuals respond to opioid overdose. The close interaction between respiratory and cardiovascular signals further complicates the investigation of mechanisms underlying bradycardia, hypoxia, and hypotension resulting from opioid overdose. To gain insight into the transient dynamic response of opioid toxidromes, we conducted experiments using a porcine model, chosen for its physiological similarities to humans in terms of the cardiovascular and pulmonary systems.[30,31] In Figure 2A, we illustrate a swine subjected to two sequential administrations of fentanyl. After the initial fentanyl administration, which resulted in RD but not overdose, we observed a sudden reduction in HR with an onset time of 21 s, preceding the development of RD. The HR reached a nadir before the RR plateaued, with a decrease in HR from 85 beats per minute (BPM) to 44 BPM lasting approximately 310 s. Subsequently, 132 s after the administration of fentanyl, the RR started to decrease gradually from 31 breaths per minute (bpm) to 14 bpm over 241 s, maintaining a plateau until the administration of the second dose of fentanyl. Concurrently, SpO_2 slowly dropped from 95% to 85% after the onset of RD, taking 300 s, and then more rapidly from 85% to 65% during the slowed RR plateau, lasting 192 s. Notably, blood pressure remained relatively stable during the opioid poisoning phase.

Following the second fentanyl administration, which induced an acute overdose, RA commenced 39 s later, leading to a rapid drop in SpO_2 from 67% to 10% with a duration of 37 s. Interestingly, we observed a gradual increase in HR that happened 97 s before the second fentanyl administration and a rapid increase in HR after the onset of RA, which could be attributed to hypoxia or a self-recovery response to fentanyl poisoning. To prevent fatality and violating animal ethics, we supplied pure oxygen to the animal immediately after SpO_2 reached 10%. This resulted in a quick recovery of blood pressure just seconds after the onset of hyperoxia, with HR peaking as SpO_2 reached 100% before declining once again. We speculate that the initial HR increase could be attributed to the hypoxia, while the subsequent decrease may be linked to the supply of 100% oxygen, causing hyperoxia and a toxic cardiovascular effect. Additional data regarding fentanyl overdose with various testing conditions are presented in Figure S3. In Figure S3A, we depicted an acute overdose scenario without the administration of 100% oxygen. The SpO_2 and blood pressure became undetectable 94 and 160 s after the fentanyl administration, respectively. Unfortunately, due to the lack of detectable cardiovascular signals via the oximeter and arterial line, we were unable to observe an increase in HR after it plateaued. Notably, the time of onset to a decrease in HR was 6 s after fentanyl administration, which is considerably faster than the onset of RD at 29 s. Although the slowed HR occurred before the development of RD, there was no bradycardia (HR < 60 BPM) after the HR reached a plateau. Blood pressure started to drop immediately after the decrease in SpO_2.

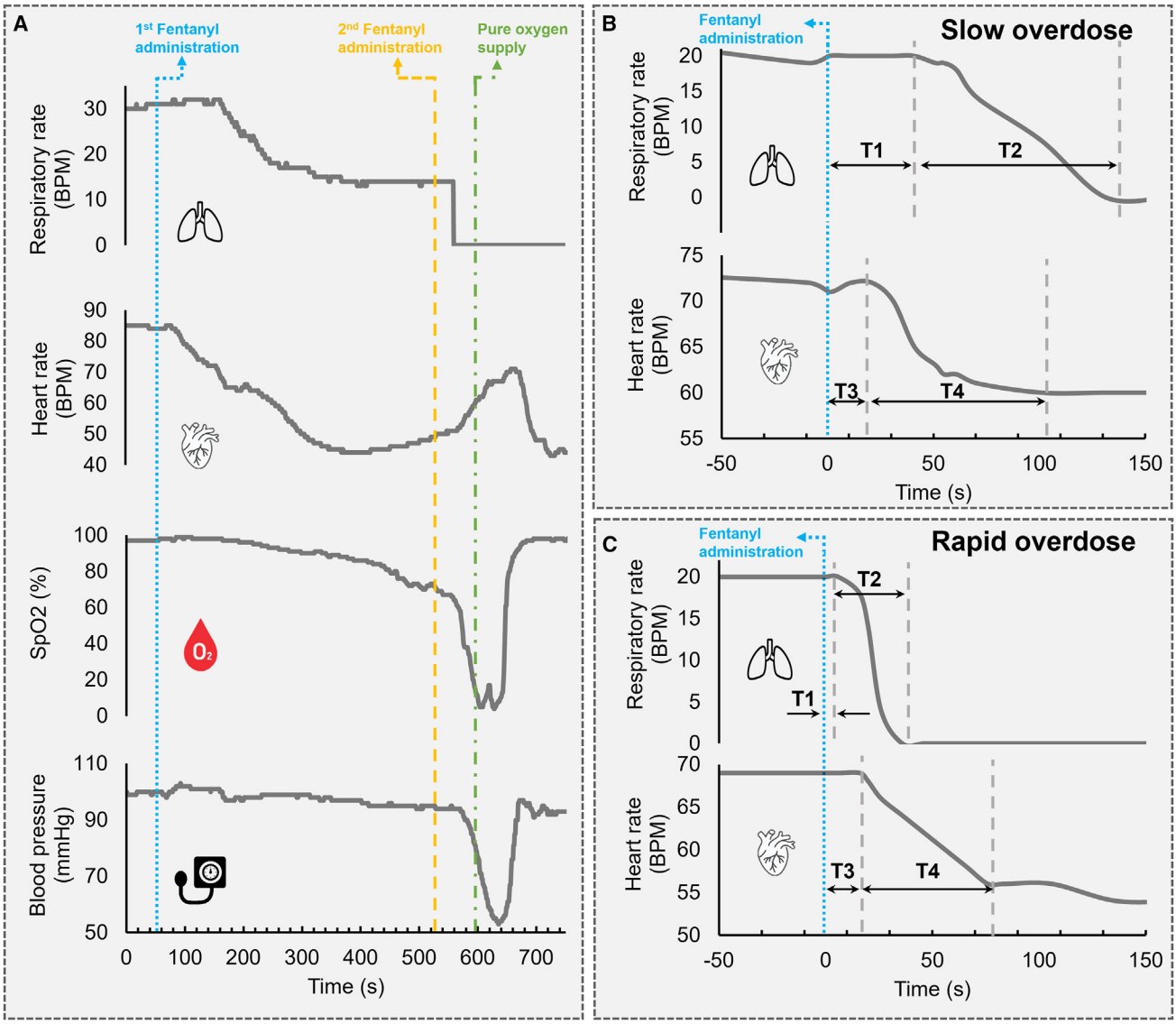

Figure 2. Transient dynamic response to fentanyl overdose, examining coupled and decoupled cardiorespiratory signals

(A) Swine RR, HR, oxygen saturation, and blood pressure during two consecutive fentanyl administrations with medical air supply

(B and C) Decoupled respiratory and cardiovascular signals, representing (B) slow and (C) rapid overdose scenarios using pure oxygen supply (100% oxygen). Key time points include T1, onset time of respiratory depression (RD); T2, duration of RD; T3, onset time of HR decrease; and T4, duration of HR drop.

In Figure S3B, we illustrate an acute overdose condition with assisted ventilation and 100% oxygen supply after severe hypoxia (SpO_2 < 20%). Surprisingly, the HR started to decrease almost simultaneously with RR. RA occurred immediately when the RR started to drop, and the HR took 28 s to reach a plateau. Blood oxygenation and blood pressure also started to drop immediately after the onset of RA. The SpO_2 decreased from 90% to 20% in 70 s. Notably, the initial blood pressure of the pig before fentanyl administration was lower (45 mm Hg) than in the other cases. After 150 s of fentanyl administration, the blood pressure dropped to zero in 105 s. Manual ventilation was performed using a bag valve mask with a frequency of 10 breaths per minute when SpO_2 dropped below 20%, resulting in a rapid increase in SpO_2 and a subsequent decrease in HR. Assisted ventilation did not mitigate the decrease in blood pressure. Subsequently, 100% oxygen was supplied, and despite an initial 30-s drop in SpO_2, it increased again until reaching 100%. The supply of 100% oxygen led to a gradual increase in HR followed by a rapid decrease, and the blood pressure started to recover when SpO_2 reached 80%, resembling the responses shown in Figure 2A.

Collectively, the data presented in Figures 2A and S3 suggest that hypoxia is an outcome of RD and that it is intensified by the presence of RA and that hypotension is primarily induced by severe hypoxia, which limits their utility as early detection biomarkers for opioid overdose. It has also been reported clinically

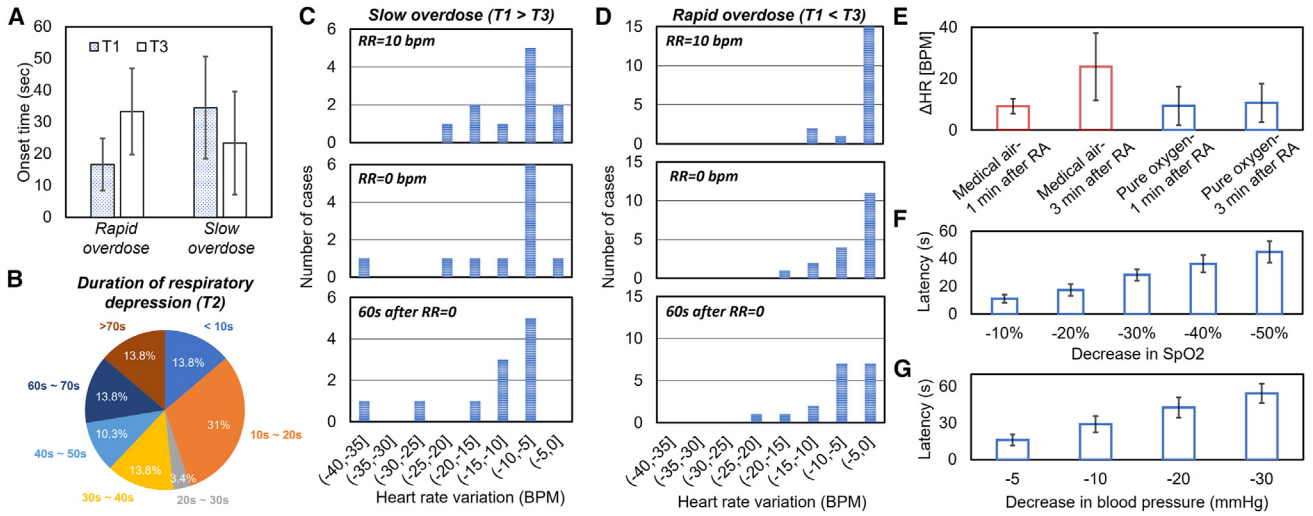

Figure 3. Characterization of the dynamics of the opioid toxidromes

(A) The onset time of RD (T1) and slowed HR (T3) of 12 pigs classified as slow overdose and 17 pigs classified as rapid overdose. All pigs received the same fentanyl dose.

(B) Distribution of the duration of RD (T2).

(C and D) The distribution of HR variation of the overdosed pigs with the decrease of HR developing (C) earlier and (D) later than RD captured at various time points (RR = 10 bpm, RR = 0 bpm, and 60 s after RR = 0 bpm).

(E) Decrease in HR of overdosed pigs with medical air and pure oxygen supply captured 1 min and 3 min after the onset of RA (medical air group, $n = 3$; pure oxygen group, $n = 29$).

(F) The latency of the drop in oxygenation after the onset of RA ($n = 3$).

(G) The latency of the drop in blood pressure after the onset of RA ($n = 3$).

that the cardiorespiratory signals are strongly coupled, particularly at RR levels below 10 bpm. Consequently, the dynamic response of cardiovascular signals during opioid overdose resembles that observed in sleep apnea and intentional breath holding scenarios. Note S1 discusses how RD and RA affect HR in the setting of sleep apnea and intentional breath holding. Figures S4 and S5 show the respiratory signal and HR of three patients from the OSASUD dataset[32] with sleep apnea. Tables S1 and S2 statistically show HR variation during sleep apnea. In contrast, the rapid decrease in HR observed prior to the onset of RD may hold promise as a potential early detection sign for opioid overdose. Decreased HR is not only the consequence of RD but also a direct toxic effect to the cardiovascular system. To further investigate whether the rapidly decreased HR is independent of respiratory signals and how much opioid directly contributes to it, the cardiovascular signal must be separated from the respiratory signal. Fortunately, clinical evidence supports the use of 100% oxygen to effectively decouple respiratory and cardiovascular signals, thereby preventing bradycardia and tachycardia from being apneic events.[33]

Decoupled cardiorespiratory signals during fentanyl overdose

Figures 2B and 2C depict the two most representative dynamic responses to slow and rapid opioid overdose in pigs receiving 100% oxygen during sedation. It is important to note that, in the presence of 100% oxygen supply, both SpO_2 and blood pressure remain constant and, therefore, are not presented here. Due to variations in individual fentanyl pharmacokinetics, the degree of overdose differs among the pigs, resulting in varying speeds of transition from fentanyl administration to the onset of RD and RA. In cases of slow overdose (Figure 2B), a prolonged onset time of RD (denoted as T1) is expected, with the duration of RD (T2) typically exceeding 1 min. In contrast, the onset time of HR decrease (T3) and its duration (T4) are shorter than those of RD. Rapid overdose scenarios (Figure 2C) exhibit a quick onset and shorter duration of RD. Overall, we conducted experiments involving 29 pigs supplied with 100% oxygen during the overdose period, and their cardiorespiratory signals are detailed in Figure S6.

Figure 3A provides insights into T1 and T3 across 30 pigs. In the case of slow overdose, where T1 > T3, T1 is 34.5 ± 13.6 s, while T3 is 23.3 ± 16.2 s. In terms of rapid overdose, where T3 > T1, T1 is 16.6 ± 8.2 s, while T3 is 33.3 ± 16.1 s. The T1 and T3 of each pig are described in Figure S7A. Figure 3B presents an overview of the duration of RD, starting from the decrease in RR until the onset of RA. Among the 29 pigs, most of them (72.4%) experienced RR decreases to zero within 60 s after the onset of RD. Furthermore, 13 pigs (34.8%) reached RA in under 20 s after the onset of RD, with four pigs (13.8%) even progressing to RA in less than 10 s.

Figure 3C and 3D showcase HR variations in pigs receiving 100% oxygen with T1 > T3 and T1 < T3, respectively, captured at different time points: RR = 10 bpm, RR = 0, and 60 s after RR = 0. For cases where T1 > T3 ($n = 11$), at RR = 10 bpm, 9 cases exhibited HR drops of more than 5 BPM. At RR = 0, 10 cases displayed HR drops of more than 5 BPM, with one case experiencing a drop of over 35 BPM. At 60 s after RR = 0, all

cases demonstrated HR drops more than 5 BPM. Conversely, for cases with T1 < T3 (Figure 3D, n = 18), only 3 cases saw HR drops of more than 5 BPM at RR = 10 BPM. At RR = 0, 7 cases had HR drops of more than 5 BPM, which increased to 11 cases at 60 s after the onset of RA. Unlike the slow overdose cases (T1 > T3), there are still 7 pigs with less than a 5-BPM drop in their HR at 60 s after the onset of RA in the cases of rapid overdose. Overall, there are 35% that develop a HR decrease prior to RD, 41% displaying an HR drop of at least 5 BPM at RR = 10 bpm, 59% experiencing an HR drop of at least 5 BPM at the onset of apnea, and 76% showing an HR drop of at least 5 BPM 1 min after the onset of RA (Figure S7B). The results depicted in Figures 3A–3D suggest that detecting T1 > T3 and observing an HR drop of more than 5 BPM at RR = 10 bpm can serve as early detection indicators of opioid overdose. In the presence of pure oxygen supply, respiratory signals are decoupled from cardiovascular signals; therefore, the reduction in HR is exclusively the direct contribution of the opioid-induced cardiovascular toxic effect.

Figure 3E summarizes the variation in HR reduction among pigs supplied with medical air (21% oxygen) and 100% oxygen at different time points. Notably, there is no difference in the HR decrease in pigs receiving 100% oxygen between 1 and 3 min following the onset of RA. Pigs supplied with medical air exhibit a similar HR reduction 1 min after the onset of RA compared to those receiving pure oxygen. However, the HR reduction in pigs receiving medical air 3 min after RA is significantly higher than in all other cases. These findings highlight the acute impact of opioids on cardiovascular signals, with onset occurring within 1 min after the occurrence of RA. Meanwhile, the coupling effect of cardiorespiratory signals predominantly manifests around 1 min after RA. In Figure 3F, the reduction time of hypoxia from −10% to −50% after the onset of RA is depicted. The reduction speed of SpO_2 remains almost constant, averaging about −1%/s. Figure 3G illustrates the latency of blood pressure drop, indicating that it takes approximately 15 s after RA to observe a 5-mm Hg reduction in blood pressure, about 42 s for a 20-mm Hg drop, and 55 s to reach a 30-mm Hg reduction. The reduction rate of blood pressure gradually increases as hypotension is primarily induced by hypoxia, emphasizing that the more severe the hypoxia, the faster the onset of hypotension. In addition to the cardiorespiratory signals, Figure S7C also demonstrates the temperature variation in response to opioid overdose. It took more than 5 min to see a 0.2°C drop.

Spatial investigation of various sensors

The iSOS incorporates three different types of sensors (electrical, optical, and mechanical) to capture various cardiorespiratory signals. It is known that electromechanical signal quality is closely related to the positioning of the sensors relative to the signal sources. For example, loop recorders are typically implanted s.c in the chest, directly on top of the heart, to ensure reliable detection of electrical pulses.[29] Researchers have also demonstrated that wearable accelerometers can effectively capture the mechanical movement induced by respiration at the abdomen.[34] Additionally, PPG sensors, commonly used in hospitals, are placed on fingertips to measure blood oxygen levels and HR via the difference in the optical absorption between oxygenated and deoxygenated blood cells.[35] These sensors are optimized for specific body sites to achieve optimal performance.

Once the multi-sensing modality was integrated into a single unit, the following question arose: where is the best location to host the integrated unit? To answer this question, we placed the sensor array at various locations and orientations s.c on the chest and abdomen. We first recorded and analyzed the signal intensity and signal-to-noise ratio (SNR) of RR and HR captured by the s.c. implanted ECG. There was no significant difference in the signal intensity of the ECG QRS peak in the chest, regardless of orientation (Figure S8). It is not surprising that the QRS peak is stronger in the left thoracic cavity compared to the right. However, it is surprising that the ECG signal in the s.c. abdomen is still easily detectable, although with about half the amplitude of that measured at the chest (Figure 4A). Importantly, the QRS peak is only detectable in the s.c. tissue and not on the skin at the abdomen.

Figure 4B demonstrates that the SNR of respiratory signals measured at the abdomen is higher than that of the chest. Unlike ECG and IMU, PPG is not sensitive to location and orientation in either the chest or abdomen (Figure S9). PPG measures light variation caused by hemoglobin absorption. Different light wavelengths contribute differently to cardiorespiratory signals, as shown in Figures 4C and 4D. In terms of respiratory signals, the SNRs of light with different wavelengths are all higher than 2, with that of red light being significantly higher than those of the other two. In terms of the cardiovascular signal, the SNR of infrared (IR) light is the highest. The raw and filtered signals obtained from each type of sensor can be found in Figure S10.

Considering the favorable acceptability of cardiorespiratory signals measured at the abdomen, we further investigated the accuracy of RR and HR estimations (Figure S11). For RR estimation, the IMU exhibited the lowest mean error of 0.06 bpm, with a standard deviation of 1.2 bpm. PPG had a mean error of 0.25 bpm and a standard deviation of 1.27 bpm. ECG showed the highest error for RR estimation, with a mean error of 0.47 bpm and a standard deviation of 2.18 bpm. Error analyses of HR estimation using ECG demonstrated the lowest mean error of 0.07 BPM, with a standard deviation of 1.07 BPM. PPG exhibited a mean error of 0.34 BPM and a standard deviation of 0.52 BPM for the HR estimation. The representative waveforms of the cardiorespiratory signals captured by ECG, PPG, and IMU before and after an overdose for analyzing the accuracy of HR and RR can be found in Figure S12.

Trade-off between detection accuracy and energy consumption with varying sampling frequency

After identifying robust physiological biomarkers for detecting overdose and determining the optimal location for capturing these biomarkers, the next step is to implement continuous monitoring of cardiorespiratory signals for real-time overdose detection. However, continuous monitoring poses a challenge due to the high power consumption of multi-sensing modalities and the trade-off between energy usage and sampling accuracy. When all sensors are turned on at their highest sampling frequency for continuous monitoring, the system's battery life is

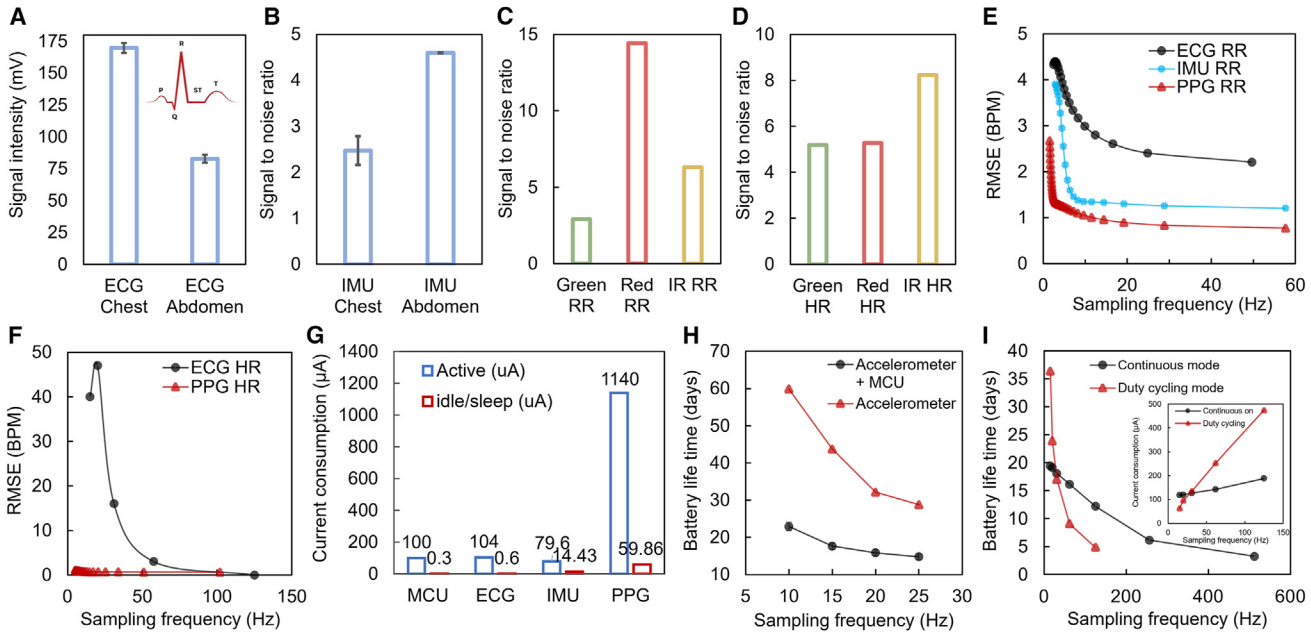

Figure 4. Spatial and temporal analyses of the capacity for real-time detection of overdose

(A) Cardiorespiratory signal intensity captured by ECG at the s.c. chest and abdomen (n = 3, repated three times on one pig).

(B) Respiratory signal intensity captured by accelerometer at the s.c. chest and abdomen (n = 3, repeated three times on one pig).

(C and D) Cardiorespiratory signal intensity captured by PPG in the s.c. chest with the orientation facing toward muscle and skin for (C) RR and (D) HR analyses.

(E) Root-mean-square error (RMSE) analyses of HR captured by ECG and PPG at the s.c. abdomen by varying the sampling frequencies.

(F) RMSE analyses of RR captured by ECG, accelerometer, and PPG at the s.c. abdomen.

(G) Current consumption of the MCU, ECG, IUM, and PPG in active and sleep modes.

(H) Current consumption of the ECG with varying sampling frequencies and duty cycles.

(I) Current consumption of the accelerometer with varying sampling frequencies.

approximately half a day. Consequently, frequent recharging is necessary to maintain optimal performance.

To reduce energy consumption in continuous monitoring of opioid overdose, we evaluated sensor performance by varying the sampling frequency, considering that power consumption is proportional to the sampling frequency. Figure 4E presents the root-mean-square error (RMSE) analysis of each sensor for RR estimation at different sampling frequencies. The RMSE for all sensors decrease significantly with increasing their sampling frequency and level off when the frequency exceeds 10 Hz. PPG is less affected by decreasing sampling frequency, with the RMSE starting to increase noticeably below 3 Hz. At 2 Hz, the RMSE for PPG estimation reaches 2.5 bpm. The RMSE for IMU estimation of RR remains relatively constant until the sampling rate drops to 10 Hz, after which it increases, reaching 3.5 bpm at the 3-Hz sampling rate. Similarly, the RMSE for ECG estimation of RR gradually increases as the sampling frequency decreases, with the RMSE reaching 4 bpm when the frequency falls below 5 Hz.

Figure 4F displays the RMSE of HR estimation via ECG. At the 64-Hz sampling frequency, the RMSE is close to zero. However, the error increases significantly as the sampling frequency decreases. The on-board HR calculation becomes completely inaccurate when the sampling rate falls below 40 Hz, which is captured by the Nyquist theorem. Since the frequency spectrum of the QRS complex spans about 8–20 Hz, the Nyquist theorem demands a sampling of the signal at least 2-fold of the highest frequency component. The RMSE for HR estimation using PPG remains relatively stable with decreasing sampling frequency, maintaining at 0.7 BPM when the sampling rate is above 15 Hz. At the 5-Hz sampling frequency, the RMSE is approximately 1 BPM. Table S2 provides a summary of the minimum sampling frequency of each sensor to support continuous monitoring. This knowledge enables us to dynamically adjust sensor parameters, striking a balance between detection accuracy and energy consumption.

Figure 4G summarizes the current consumption of the MCU, ECG, IMU, and PPG in active and idle/sleep modes. Figures S13–S15) detail the current consumption during sleep of the ECG, PPG, and IMU with and without waking up MCU, respectively. PPG exhibits a current consumption that is at least 10 times higher than the others in the active mode, making it unsuitable for continuous monitoring but suitable for cross-validation to conserve energy. Figures S16 and S17 show the characterization of PPG signal quality and current consumption with varying pulse widths and sampling frequencies. The current consumption of ECG is slightly higher than that of the IMU in active mode but significantly lower in idle mode. This suggests that ECG can save substantial energy by transitioning to idle mode. It is worth noting that the MCU consumes a comparable amount of current to read out sampled data from sensors and compute vital sign estimations. Fortunately, the MCU's idle current is

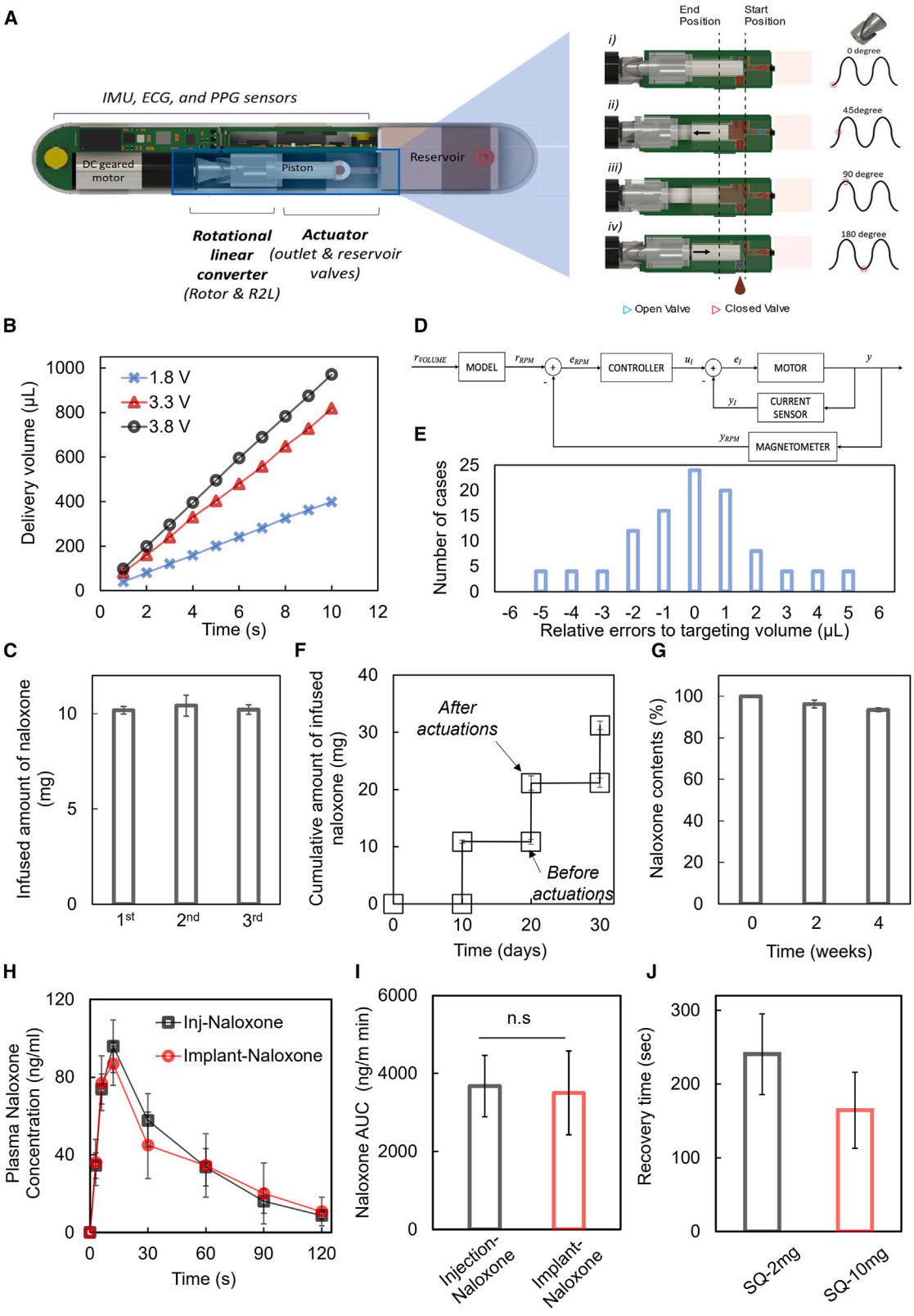

(legend on next page)

low. To reduce overall energy consumption, the MCU's wake-up frequency for sampling and data processing will be reduced.

Figure 4H illustrates the battery life needed to support continuous operation of the accelerometer at various sampling frequencies, ranging from 10 Hz to 25 Hz. We observe that the battery life of the accelerometer alone decreases as the sampling frequency increases. At a 10-Hz sampling frequency, the battery life can extend up to 60 days. However, this calculation does not account for the energy consumption of the MCU required to read out data from the accelerometer and estimate RR. When considering the combined energy consumption of the accelerometer and MCU for RR estimation, the battery life drops to 22 days at a 10-Hz operation frequency. Increasing the sampling frequency may reduce the RMSE, but it significantly decreases the battery life.

In Figure 4I, we examine the battery life of ECG at different sampling frequencies and operating modes. The continuous mode implies that the ECG remains active, while the MCU alternates between active and idle modes to read out data. In the duty cycling mode, both MCU and ECG switch back and forth between idle and active mode at the same frequency. The sampling frequency is determined by the MCU's wake-up frequency. In the duty cycling mode, the current consumption is preserved, leading to longer battery life when the sampling frequency is below 30 Hz. However, the continuous mode starts to consume less current than the duty cycling mode when the sampling frequency exceeds 40 Hz. This higher current consumption in the duty cycling mode arises from the fast switching of the ECG between active and sleep modes, requiring additional energy for the MCU to activate and deactivate the ECG. In the duty cycling mode, the ECG can achieve a maximum frequency of 128 Hz. In the continuous mode, the sample frequency can reach to 512 Hz. For RR estimation, a sampling frequency of 20 Hz can be set in the duty cycling mode, maintaining both accuracy and a battery life of 24 days. However, when capturing HR with a sampling frequency of 64 Hz, the continuous mode results in a battery life of 16 days for the ECG. It is noteworthy that the ECG features an internal function capable of independently calculating the R-R interval, operating at 512 Hz and only requiring the MCU to wake every second to receive the value (Table S3). With an average current consumption of 135 μA, the battery life is 15 days. According to the Centers for Disease Control and Prevention, for acute pain unrelated to surgery or major trauma, providers should prescribe no more than a 7-day supply.[36] Therefore, iSOS has sufficient battery life to support continuous monitoring for real-time overdose detection. Additionally, the iSOS can be recharged when the user obtains a new prescription.

To facilitate sustained continuous monitoring, the iSOS needs recharging every 2 weeks through wireless power transfer. Figure S18 presents the *in vivo* wireless charging characteristics of the batteries. With a capacity of 55 mAh, it takes approximately one and a half hours to fully charge the battery. The transmitting and receiving coils are separated by skin with a thickness of about 3 mm.

Rapid reversal of opioid overdose

When the iSOS identifies a potential overdose, it triggers an alarm using auditory and tactile signals while simultaneously sending an alert to the user's smartphone. This alert provides users with the opportunity to override the decision for naloxone administration in the event of a false-positive detection. Following this, a large bolus of naloxone is rapidly infused using a DC-brushed motor and two-valve-based actuator. This actuator transforms a single revolution of the motor into double the linear actuation, as shown in Figures 5A and S19 and Video S1. Initially, (1) the piston is at the end of its path, with both the drug reservoir and outlet valves closed (0° of the rotor). (2) The piston then moves backward (45°), opening the reservoir valve and drawing the drug solution from the drug reservoir. At this point, the outlet valve remains closed. (3) Once the piston reaches its furthest position (90°) and the required amount of drug has been drawn, both valves close again. (4) Finally, as the piston returns to its starting position (180°), the reservoir valve stays closed while the outlet valve opens, allowing the drug to be infused into the body.

By actuating the DC motor with a speed of 500 rpm, the pump can achieve 1,000 actuations per minute. The volume of infusion corresponding to the number of actuations is detailed in Figures S20 and S21 as well as Note S2. The infusion volume can be adjusted by varying the driving voltage of the DC brushed motor. Consequently, at a voltage of 3.8 V, the pump is capable of infusing 1,000 μL of naloxone in a mere 10 s, as illustrated in

Figure 5. Rapid on-demand delivery of naloxone for timely overdose rescue

(A) Main components of the device and working principle of the energy-efficient rapid drug delivery mechanism. In the initial position (0°), the piston is positioned at the end of its path, and both valves (drug reservoir and outlet) are closed. The piston moves backward (45°), while the reservoir valve opens and draws the drug from the reservoir. The outlet valve is closed. The piston reaches its farthest position (90°), and the designated quantity of the drug has been drawn. Both valves are again closed. As the piston moves back to the initial position (180°), the reservoir valve remains closed, while the outlet valve is open, releasing the drug into the body.

(B) Characterization of the controlled drug release rate with varying pump driving voltages.

(C) Infused amount of naloxone for 10 s. The devices (n = 3) were each actuated three times while being fully immersed in PBS (pH 7.4) at 37°C.

(D) Block diagram of the closed-loop controller for optimizing the energy consumption for rapid delivery of naloxone.

(E) Error distribution of the drug delivery device with the closed-loop controller.

(F) Stability assessment of naloxone in the device: The naloxone-loaded devices (n = 3) were stored at 37°C for 28 days, after which the solution in each device was extracted and compared with a fresh drug solution (n = 3).

(G) Long-term profile of naloxone infusion. The naloxone-loaded devices (n = 3) were each actuated at 10, 20, and 30 days while being fully immersed in PBS (pH 7.4) at 37°C for 30 days. There was no release of naloxone when the device was not operated.

(H) Pharmacokinetic profiles of naloxone.

(I) The AUC was calculated using the trapezoidal rule.

(J) The onset time of naloxone via s.c. administration with doses of 2 mg and 10 mg. Data are mean ± SD.

Figure 5B. This is compared to other opioid reversal devices, which administer 0.8 mg of naloxone without solid formulation over 60 s (Table S4). To evaluate the pump performance, we operated three pumps with an identical design to release the drug for 10 s. With each operation, a predetermined amount of naloxone was released (10.27 ± 0.39 mg per operation), demonstrating the device's ability to infuse an accurate volume of liquid in an open-loop control manner. Upon operation, a reproducible profile of drug infusion could be maintained until approximately 85% of the naloxone was consumed. Since the drug reservoir was made of a flexible material that prevented negative pressure build-up, the reproducibility was not affected after drug replenishment, enabling semi-permanent use following implantation (Figure 5C). To further increase the drug release accuracy, we incorporated a closed-loop controller that continuously monitors motor movement and current draw to ensure reliable naloxone delivery from the s.c. implanted pump. Motor movement is monitored using a linear magnetic encoder consisting of two hall-effect sensors and a magnet attached to the linear actuator. The control block diagram is illustrated in Figure 5D. Figure 5E illustrates the error distribution of the closed-loop controlled pump when the reference pumping volume is 200 μL. Over 100 cycles of pumping 200 μL, the maximum error remains below 2.5%, and the error is less than ±1 μL nearly 24 times. To assess the feasibility of long-term use of the system, we fully immersed the device in PBS for 4 weeks and operated it at scheduled times. The device released a reproducible amount of naloxone only when operated (10.39 ± 0.66 mg per operation), and no drug leakage was observed between operations (Figure 5F). To evaluate naloxone stability in the iSOS, we filled the drug reservoir with 1.2 mL of a solution of naloxone and operated the device under *in vitro* conditions. During the 4-week period, we observed that the stability of naloxone, with a concentration of 10 mg/mL in the reservoir, was well maintained at 37°C (Figure 5G).

As depicted in Figure 5H, the maximum plasma concentrations of naloxone for both the iSOS and injection groups were comparable: 86.9 ± 11.1 ng/mL and 95.9 ± 13.5 ng/mL, respectively. The maximum concentration time was observed to be 12 min for both groups. The area under the curve (AUC) for plasma naloxone concentration was 4,374.9 ± 1,340.1 ng/mL*min and 4,596.0 ± 983.7 ng/mL*min for the iSOS and s.c. injection groups, respectively, which were not significantly different (Figure 5I). The s.c. administered naloxone takes about 12 min to reach its maximum blood concentration, and it takes 5 min to reach 75% of its maximum value. Figure 5J demonstrates the recovery time from an overdose using the iSOS with varying doses of naloxone. The administration of 2 mg of naloxone s.c. necessitates an average recovery time of 240.6 ± 54.6 s (n = 3). Elevating the dose from 2 mg to 10 mg reduces the average recovery time to 152.0 ± 37.5 s (n = 12). As shown in Figure S22, intramuscular (i.m.) administration of 10 mg naloxone further reduces the recovery time to 91 s (n = 4). Importantly, the s.c. administration of 10 mg naloxone achieves a recovery time equivalent to i.m. administration of 0.4 mg (172.0 ± 22.7 s). For reference, intravenous (i.v.) administration of 0.4 mg naloxone results in a recovery time of 52 ± 20.2 s (n = 6), which is consistent with clinically reported data. Overdose recovery is defined as the detection of spontaneous respiration. The results depicted in Figures 5H–5J suggest that iSOS could effectively prevent not only death but also permanent brain damage and facilitate overdose recovery, as it takes approximately 10 s to completely deliver 10 mg of naloxone and recover from an overdose within 3 min. Table S5 briefly summarizes the clinically reported cases of the onset time and duration of naloxone via various administration routes.

Automated recovery of opioid overdose

Given our understanding of the transient response to fentanyl overdose, the balance between energy efficiency and overdose detection accuracy, as well as the advancement of rapid naloxone delivery mechanisms, we can now assess the performance of iSOS in real-time overdose detection and swift recovery without the need for human intervention. Figure S23 illustrates the decision-making process embedded within the iSOS. Continuous operation of the accelerometer with a low sampling frequency and ECG R-R interval detection ensures the real-time monitoring of decreased HR and RD. Upon detection of decreased HR and an RR drop of over 2 bpm, the accelerometer's sampling frequency is heightened, and the MCU takes control of ECG to acquire precise RR and HR measurements. Additionally, the PPG is activated. If a monotonous drop of HR by more than 5 BPM and RR decreasing to 10 bpm is observed, then the buzzer and vibrator are triggered to signal the delivery of naloxone. After 10 s (if T1 > T3) or 30 s (if T1 < T3) without a response, naloxone is administered. The iSOS system classifies slow and rapid overdoses by detecting the time interval during which the HR decreases by more than 2 BPM and the RR decreases by more than 5 bpm. If the time for the HR to drop by 2 BPM is shorter than the time for the RR to drop by 5 bpm, iSOS classifies it as a slow overdose. We validated iSOS using recorded overdose data from clinical monitors. Among 13 cases identified by human experts as slow overdoses, iSOS correctly classified all 13. For 17 cases identified as rapid overdoses by human, iSOS correctly classified 15. Thus, the overall classification accuracy of iSOS is 93%.

Figures 6A and 6B display RR and HR data computed by iSOS and transmitted wirelessly to a laptop, indicating when overdose is detected, the medical alarm is activated, and naloxone delivery is completed. These figures represent two representative overdose cases, slow overdose and rapid overdose, showcasing real-time detection and automated recovery with iSOS. RR and HR data from iSOS are updated every 5 s via Bluetooth transmission. In Figure 6A, a ΔRR of more than 5 bpm is detected at t = 115 s, and a ΔHR of more than 5 BPM is detected at t = 95 s, classifying the case as a slow overdose. The medical alarm activates immediately upon detecting RR < 10 bpm and lasts for 10 s. Simultaneously, HR steadily decreases with a ΔHR of 15 BPM until the medical alarms cease. Naloxone delivery is initiated at t = 130 s and completed 25 s after the onset of RA. HR starts to rise at t = 200 s, and spontaneous breathing is observed at t = 220 s. Recovery takes approximately 80 s, with a 105-s duration of RA.

As shown in Figures 6A and 6B, ΔRR of more than 5 bpm is detected at t = 90 s, and a ΔHR of more than 5 BPM is detected at t = 125 s, classifying the case as a rapid overdose. The medical alarm is triggered upon detecting RR = 10 bpm and lasts for 30 s.

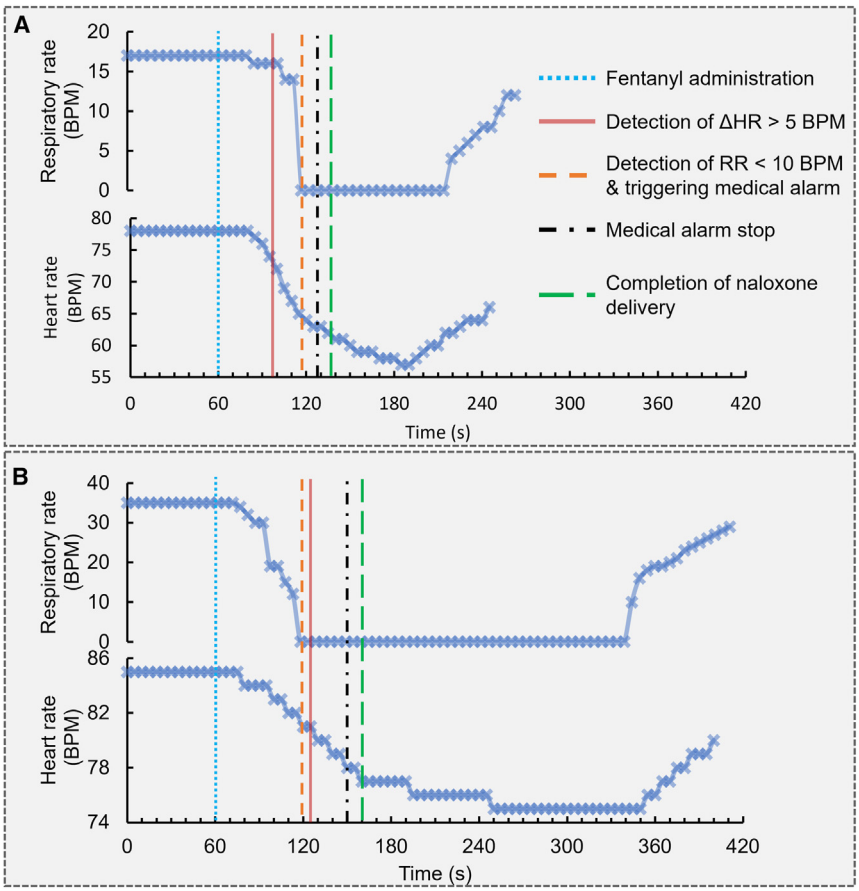

Figure 6. Automated recovery from overdose via the robotic first responder

On-board computation of RR and HR enables real-time detection of overdose and automatic delivery of naloxone in the condition of (A) T3 > T1 and (B) T1 > T3.

Simultaneously, HR monotonically decreases with a ΔHR of 7 BPM until the medical alarm deactivates. Naloxone delivery begins at t = 150 s and is completed by t = 160 s, approximately 40 s after the onset of RA. Spontaneous breathing is observed at t = 345 s, and HR starts to increase at 355 s, immediately following the recovery of respiration. The recovery phase lasts approximately 185 s, with a 245-s duration of RA. The results presented in Figure 6 demonstrate that the developed iSOS, equipped with our decision-making algorithm, effectively detects various overdose conditions in real time and initiates recovery within 5 min after RA onset, thereby mitigating the risk of permanent brain damage.

DISCUSSION

Previous attempts at developing wearable or semi-implantable systems to respond to opioid overdose have experienced challenges in compliance with wearables and noise associated with physiologic data obtained through a wearable system. While implantable systems have their own challenges, we modeled our system on other implanted devices mirroring a simple minimally invasive procedure that clinicians could perform under local anesthesia. Our iSOS is inspired by the course of clinical care for patients with OUD as a tool to support individuals in treatment by detecting and preventing overdose and as a future device for harm reduction among individuals who are at high risk of overdose. By implanting the system, we reduce the potential for device noncompliance, facilitate continuous monitoring, and provide support for individuals who may continue to use opioids alone, preventing fatal overdose. By increasing battery life as well as facilitating contactless recharging and replenishment of the naloxone reservoir during clinical visits, the iSOS integrates into traditional substance use disorder clinics and may help support individuals during the time when they are at highest risk of overdose. Extended battery life and a refillable drug delivery reservoir and pump allow the device to reside in the body long term as individuals recover and undergo OUD treatment. Conceptually, patients could receive the system at a clinic visit, where implantation could be completed at the bedside with local anesthesia. At subsequent follow-up visits, the device could then be charged wirelessly, the naloxone reservoir replenished (if necessary), and data from the system queried to inform clinicians of opioid use events and counsel patients on overdose risks in the context of ongoing treatment. As the naloxone stability stored at body temperature can last for more than 2 weeks and the battery life for supporting continuous monitoring is 16 days, it is recommended for the user to have regular clinical visits every 2 weeks. The visit frequency to the hospital can be further reduced via new naloxone formulations and the power consumption optimization for continuous monitoring. Impressive battery life has been demonstrated in loop recorders, which can continuously monitor heart activity for over 3 years without requiring recharging. This exceptional power efficiency can be attributed to a custom-designed circuit that incorporates ECG sampling, analog/digital signal processing, on-board computation, and power management into a single chip using system-on-chip (SoC) technology. To showcase this capability, we successfully showcased the ECG chip's internal capability to independently calculate the R-R interval at a sampling frequency of 512 Hz, consuming an average current of only 135 μA.

In terms of real-time detection of overdose, therapeutic drug monitoring is one potential method that was considered in the beginning of the work. However, the illicit use of a wide variety of opioids, including multiple subspecies of fentanyl (e.g., acetyl fentanyl, carfentanil, and butyrylfentanyl), complicates drug

detection and makes this approach impractical. Furthermore, drug concentrations in individuals with OUD do not reliably indicate overdose, as tolerance can lead to higher drug levels without resulting in overdose. Conversely, individuals in recovery may overdose during relapse even with a lower dose that might not be detected by drug monitoring. Physiological signals of overdose, on the other hand, are unequivocal and provide a reliable indication that an overdose has occurred, regardless of the opioid dose used.

Prompt administration of naloxone is the key to rescue victims from overdose. Although i.v. administration can quickly reach onset, the lengthy preparation requires first responders to be trained. Autoinjectors are designed to facilitate the administration process by means of a pre-filled naloxone cartridge and pre-loaded spring mechanism. However, a major drawback of naloxone autoinjectors is their reliance on a first responder to perform the administration. To address this issue, Chan et al. have developed a wearable autoinjector with an added servo motor that automatically triggers the injection.[23] The decision to deliver naloxone is based on readings from a wearable accelerometer that detects apnea. Unfortunately, the wearable autoinjector presented by Chan et al. takes over 9 min to release 3 mL of naloxone at a concentration of 0.4 mg/mL. Similarly, the hypoxia-driven wearable autoinjector designed by Imtiaz et al. takes approximately 5 min to deliver 1 mL of antidote at a concentration of 1 mg/mL. Additionally, the s.c. implantable drug delivery device developed by Dhowan et al.[13] takes more than 10 min to fully release 8.8 mg of naloxone in powder formulation, and powder formulations typically have longer absorption times in the body. Our novel delivery mechanism allows us to solve this engineering challenge by significantly expediting the release of a large bolus of concentrated naloxone. Our pharmacodynamic studies suggest that increasing the naloxone dose can expedite the onset of action. The Rapid Opioid Countermeasure System with a total naloxone dose of 10 mg and concentration of 10 mg/0.4 mL is specifically designed for military personnel and chemical incident responders for rapid recovery from an overdose, and it received US Food and Drug Administration approval in February 2022. However, it is recommended to be stored at room temperature to maintain stability. Therefore, the concentration used in this work is fixed at 10 mg/mL, as a higher concentration usually results in lower stability.

The current iteration of iSOS utilizes a polymethylmethacrylate outer surface uniformly coated with Parylene C to enhance biocompatibility.[37] Future iterations should consider employing high-strength materials such as titanium, stainless steel, or liquid crystal polymer.[38] Additionally, encapsulating the device with soft biomaterials that emulate tissue properties, such as silicone elastomer, polyurethane (PU), or epoxy, should be considered. This strategy can minimize the mechanical modulus mismatch at the interface between the implant and biological tissues while concurrently minimizing fibrotic capsule formation.[39]

Although iSOS shares a similar form factor with a loop recorder, its large size can deter patients from using it due to the requirement of an invasive surgical procedure. The drug delivery compartment takes up 70%, of which the drug reservoir accounts for around 57%. The battery takes around 20% of the space, while the emergency alert and electronics components occupy the remaining 10%. To further reduce the form factor, several approaches can be considered. First, the drug reservoir size can be decreased by introducing a new naloxone formulation with a higher concentration. Second, the battery volume can be reduced by increasing its energy density, lowering power consumption, or accepting a shorter battery life. Third, the drug delivery compartment can be made smaller by utilizing a more compact DC motor. Last, the electronics footprint can be minimized by leveraging SoC technology to integrate multiple components into a single chip. These strategies collectively aim to optimize the implant's size and enhance patient acceptance. Additionally, user acceptance and the willingness of individuals with OUD to utilize an implantable system like iSOS still needs to be explored. Future work should include mixed-methods work to compare the willingness of individuals with OUD to engage with wearable devices compared to iSOS. These key explorations may assist with strategies to discuss iSOS with potential candidate patients and to revise features of iSOS to improve acceptability among these populations.

Overall, we demonstrate the development of a novel implantable device that uniquely autonomously senses and verifies opioid overdose and, in response, rapidly delivers naloxone and monitors recovery from overdose. This is significant because of several reasons. First, no other wearable/implantable device has been demonstrated previously to adequately fuse several sensor modalities to reliably detect an opioid overdose event. Second, our *in vivo* large animal studies investigated the transient response of coupled and decoupled cardiorespiratory signals after the onset of fentanyl overdose; these studies reveal that an acute decrease in HR prior to the development of RD can differentiate overdose from other conditions, including sleep apnea and intentional breath holding. Third, iSOS incorporates an on-board algorithm based on the discovered overdose biomarkers that autonomously decides when to administer naloxone and monitors recovery, key features that other naloxone delivery or opioid overdose systems have not explored. Finally, we developed strategies to conserve battery life and allow for drug reservoir refilling that mirror the cadence of clinical visits for individuals with OUD. These innovations suggest that an implantable device like the one we present may be able to integrate into the continuum of OUD care. This pivotal work demonstrates the feasibility of developing an implantable device to support harm reduction in OUD that addresses previous challenges in other systems.

EXPERIMENTAL PROCEDURES

Resource availability

Lead contact

Requests for further information, resources, and reagents should be directed to and will be fulfilled by the lead contact, Giovanni Traverso (cgt20@mit.edu).

Materials availability

This study did not generate new unique reagents.

Data and code availability

All data are available in the main text or the supplemental information. Codes for sampling and processing data are available at https://github.com/Jhc999/iSOS.git. Additional data related to this paper may be requested from the authors. This paper does not report any original code or algorithms. Any additional information required to reanalyze the data reported in this work is available from the lead contact upon request.

Materials involved

Med 610 and Clear resin were purchased from Stratasys and Formlabs, both to be used as 3D printing materials. PU film, with a thickness of 100 μm, was purchased from Plastic Film. The one-way check valves were purchased from Minivalve. The ECG electrodes were made of copper sheets with a thickness of 0.1 mm and laser cut with user-defined shapes. The rigid printed circuit boards (PCBs) were made out of FR-4 material. The manufacturing of the FR-4 PCBs and assembly of the electronics were finished by Bittele Electronics. Medical epoxy (Epo-tek 301) was purchased from Epoxy Technology. The PCB was designed by Altium Designer. The bill of materials is listed in Table S6. Each component of the device was designed using 3D CAD software (Autodesk Fusion 360) and subsequently fabricated with 3D printers (Stratasys J850, Formlabs Form 3+, and BMF microArch S230). The circuit schematics and layout were designed via Altium and can be found in Note S3.

Ground-truth vital sign monitoring and recording

Respiratory signals, such as end tidal CO2 and RR, along with body temperature and cardiovascular signals, which include blood pressure, pulse, and oxygenation, were collected using standard clinical patient monitors. ETCO2 and RR were measured by monitoring air exchange during inhalation and exhalation through ventilation. Body temperature was acquired using a thermistor inserted into the esophagus, while blood pressure was obtained through an arterial line. SpO_2 and HR were recorded by placing an oximeter on the ear, and HRV data were captured by attaching ECG patches to the chest.

On-board sensing and computing

A microcontroller with a built-in Bluetooth module (nRF 52840) is employed for on-board signal processing and decision-making. The nRF52840 is built around the 32-bit ARM Cortex-M4 CPU with a floating point unit running at 64 MHz. A pulse oximeter (MAX 30101) with near-IR, red, and green light is used to measure the light absorption in the tissue. An analog front end (MAX 30003) is used to capture the ECG. A clinical-grade temperature sensor (MAX30208) is employed to measure body temperature. An IMU (BMX160) is employed to capture body movement and respiration-induced motion. Root-mean-square errors are calculated by comparing the s.c. implanted ECG and PPG sensor in the chest to a standard clinical vital sign monitor. The sensor readouts from ECG and PPG were recorded for 1 min at each sampling frequency, with the HR ranging between ~60–70 BPM. The HR from the implantable ECG and PPG is calculated by the on-board embedded computation unit.

Power management for the drug delivery, vital sign monitoring, and computation

One customized pin-type lithium secondary battery (46530Z, Synergy; see supplemental information for the datasheet) with a capacity of 55 mAh and a rated voltage of 3.8 V is used to provide the entire implantable system with a stable power supply. A fuel gauge (MAX 17263) and current sensor (INA 231) are employed to monitor the voltage drop and current draw of the battery. A bulk-booster converter (MAX 77643) with three independent programmable output voltages (0.8–5 V) is employed to supply a stable voltage to the microcontroller, Bluetooth communication, a variety of sensors, the pump, and the medical alert system. The Sub-Micro Plastic Planetary Gearmotor purchased from Pololu is a brushed DC motor with a gear ratio of 1:26. The operating voltage is between 0.7 V and 9 V, and the stall current is 400 mA. The current draw and speed of the motor with varying the driving voltage are shown in Figure S20. More details about the energy optimization in the battery-powered drug delivery system can be found in our previous work.[40]

In vivo wireless power system

Inductive coupling wireless powering with a resonating frequency of 1 MHz is adopted to enable *in vivo* charging of the lithium battery. The wireless charging transmitter (LTC 4125) and receiver (LTC 4124) circuitries are shown in Figure S18. The receiving coil (IWAS3010AZEB130KF1) and transmitter coil (IWAS4832AAEB220JF1) are both commercially available, and they were purchased from Mouser Electronics.

In vitro performance test

To evaluate device performance *in vitro*, we filled each of the three devices with 1.2 mL of a naloxone solution (10 mg/mL) and operated them while fully immersed in 50 mL of PBS (pH 7.4) at 37°C. *In vitro* naloxone concentrations were analyzed by high-performance liquid chromatography with ultraviolet using an Agilent 1260 Infinity system consisting of a quaternary pump, chilled autosampler, thermostatic column compartment, and diode array detector (DAD). Samples were injected at a volume of 5 μL onto a superficially porous C18 column (3.0 × 50 mm, dip = 2.7 μm), thermostatically held at 25°C, and equipped with a 5-mm-long guard column. The mobile phase consisted of 0.1% formic acid in water (v/v) (A) and acetonitrile (B), with a flow rate of 1.0 mL/min and programmed gradient of 0 min, 5% B; 3 min, 60% B; and 3.1 min, 95% B with a stop time of 7 min and re-equilibration time of 4 min. Absorbance at 282 nm with a bandwidth of 4 nm and scan rate of 5 Hz was used to detect and quantify naloxone by the DAD.

Drug refillability

To investigate the impact of drug refilling on the drug release characteristics, an iSOS containing 1 mL of naloxone solution (10 mg/mL) was submerged in PBS (pH 7.4), and we compared the pre- and post-refilling procedure (Figure 5C). The refill septum is specifically designed for facile detection on the skin above the implanted iSOS. Through this refill septum, the residual drug solution is extracted from the flexible drug reservoir and replaced with fresh drug solution using a 27G needle, all while the iSOS remains in place (Figure S24).

In vivo evaluation protocols in a swine model

All *in vivo* studies were approved by the Massachusetts Institute of Technology Committee on Animal Care. Female Yorkshire swine (Cummings School of Veterinary Medicine at Tufts University, North Grafton, USA) in the range of 60–80 kg were used for the testing of fentanyl overdose and recovery using naloxone. The animals were kept on a liquid diet for 24 h before the procedure and fasted overnight. Pigs were sedated with an i.m. injection of Telazol (2–6 mg/kg) and xylazine (2–4 mg/kg) and kept on isoflurane (2%–3%) and oxygen (100%) via endotracheal tube. For blood sampling, an indwelling catheter (Central Venous Catheter Kit, 7Fr-30CM [12″], Jorgensen Labs) was placed in the femoral vein under aseptic conditions. Two different ventilation conditions were employed. One is medical air with 21% oxygen supply, and the other one is 100% oxygen supply. Fentanyl with a concentration of 6 μg/kg was administered over 30 s via the central venous catheter. Naloxone with different concentrations and total doses was given at the abdomen via s.c., i.m., and i.v. administration as well as the s.c. implantable pump. All of these experiments were non-survival. The animals were euthanized under anesthesia with sodium pentobarbital at 100 mg/kg IV, consistent with the American Veterinary Medical Association Guidelines[41] for the Euthanasia of Animals.

Pharmacokinetic studies on naloxone delivery

To conduct the pharmacokinetic tests, we divided the Yorkshire swine into two groups: (1) animals treated with s.c. injections of naloxone (Inj-Naloxone) and (2) animals implanted with the naloxone-loaded device (Device-Naloxone), to which 10 mg of naloxone was administered via s.c. injection or operation, respectively. We collected 600 μL of blood from a central line connected to the external jugular vein or from a mammary vein into BioLegend Vacutainer gold-top tubes (Becton Dickinson, USA) 0, 3, 6, 12, 20, 60, and 120 min after administration. The plasma samples were separated from the blood by centrifugation at 3, 000 ×*g* for 10 min and stored at −80°C until measurement. The naloxone concentration in the plasma was analyzed using liquid chromatography triple-quadrupole mass spectrometry. An Agilent 1290 ultra-high-performance liquid chromatography system with a binary pump, autosampler, and thermostat was coupled to an Agilent 6495B triple-quadrupole mass spectrometer. Datasets were generated using the Masshunter Liquid Chromatography-Mass Spectrometry Control Suite, and data processing and analysis were performed in QuantMyWay. Naloxone (API) and naltrexone (ISTD) were separated on an Agilent Poroshell 120 EC-C18 analytical column, 3.0 × 50 mm with 2.7-μm particles, maintained at 40°C. The optimized mobile phase consisted of A (0.1% formic acid in water) and B (acetonitrile). Gradient elution was employed over 6 min, starting with 95% A at 0 min and ending with

5% A at 5 min at a flow rate of 0.750 mL/min. The injection volume was 2 μL. The compounds underwent electrospray ionization (positive mode) with a drying gas temperature of 250°C, sheath gas temperature of 380°C, sheath gas flow rate of 10 L/min, and drying gas flow of 16 L/min. The nebulizer was kept at 35 psi. The capillary voltage was set to 3,000 V in positive mode, and there was no in-source fragmentation. Naloxone and naltrexone were monitored under dynamic multiple reaction monitoring with transitions of 328.16 m/z → 310.0 m/z and 342.1 m/z → 324.0 m/z for naloxone and naltrexone, respectively. The collision energies were set as 12 V and 20 V for naloxone and naltrexone, respectively. A low limit of quantification of 100 pg/mL was achieved using the sample preparatory and analytical methodologies conveyed in this report. We conducted three analyses for each sample. We only considered drug concentrations as non-zero if they were above the lower limit of detection in all three analyses. In this study, we tested each group in three pigs based on our previous studies in the large animal model.

Statistical analysis

The data were presented as means ± standard deviation (SD). We performed statistical analysis using GraphPad Prism 7 (GraphPad). To compare the means of two groups, we used Student's t tests, where the differences were considered to be statistically significant when $p < 0.05$.

SUPPLEMENTAL INFORMATION

Supplemental information can be found online at https://doi.org/10.1016/j.device.2024.100517.

ACKNOWLEDGMENTS

Funding was provided by Novo Nordisk, The McGraw Family Foundation, Brigham and Women's Hospital, the MIT Department of Mechanical Engineering, and the MIT Karl Van Tassel (1925) Career Development Professorship Chair. P.C. was funded by NIH DP2DA056107.

AUTHOR CONTRIBUTIONS

Conceptualization, H.-W.H., P.R.C., S.L., and G.T.; methodology, H.-W.H., T.K., P.R.C., J.C., A.W., S.L., N.F., J.J., A.P., A.M.H., and K.I.; investigation, H.-W.H., P.R.C., S.L., T.K., J.C., I.B., and S.M.; visualization, H.-W.H., P.R.C., J.C., and T.K.; funding acquisition, H.-W.H., A.C., and G.T.; project administration, H.-W.H., P.R.C., A.C., and G.T.; supervision, H.-W.H., P.R.C., A.C., and G.T.; writing – original draft, H.-W.H. and P.R.C.; writing – review & editing, all authors.

DECLARATION OF INTERESTS

The authors declare submission of a provisional patent application (PCT/US2022/080385) describing the materials and applications of the systems described here. Complete details of all relationships for profit and not for profit for G.T. can be found at www.dropbox.com/sh/szi7vnr4a2ajb56/AABs5N5i0q9AfT1IqIJAE-T5a?dl=0.

Received: July 2, 2024
Revised: July 18, 2024
Accepted: July 25, 2024
Published: August 14, 2024

REFERENCES

1. Hedegaard, H., Miniño, A.M., and Warner, M. (2018). Drug Overdose Deaths in the United States, 1999-2017 (NCHS Data Brief), pp. 1–8.
2. Polston, G., Goyal, A., and Mechanic, O.J. (2018). Opioid Overdose. In Challenging Cases and Complication Management in Pain Medicine (Springer, Cham), pp. 3–7. https://doi.org/10.1007/978-3-319-60072-7_1.
3. Bhardwaj, H., Bhardwaj, B., and Awab, A. (2014). Revisiting opioid overdose induced acute respiratory distress syndrome. Indian J. Crit. Care Med. *18*, 119–120. https://doi.org/10.4103/0972-5229.126095.
4. Boyer, E.W. (2012). Management of Opioid Analgesic Overdose. N. Engl. J. Med. *367*, 146–155. https://doi.org/10.1056/NEJMRA1202561/.
5. O'Neill, S., Wayman, M., and Schofield, I. (2023). Hypoxic Brain Injury. CPD Anaesth. *9*, 157–159. https://doi.org/10.5772/intechopen.89487.
6. SpinalCord.com Team (2021). What You Need to Know About Brain Oxygen Deprivation. https://www.spinalcord.com/blog/what-happens-after-a-lack-of-oxygen-to-the-brain.
7. Barnett, B.S., Chai, P.R., and Suzuki, J. (2023). Scaling Up Point-of-Care Fentanyl Testing — A Step Forward. N. Engl. J. Med. *389*, 1643–1645. https://doi.org/10.1056/NEJMP2308525.
8. Nuamah, J., Mehta, R., and Sasangohar, F. (2020). Technologies for Opioid Use Disorder Management: Mobile App Search and Scoping Review. JMIR Mhealth Uhealth *8*, e15752. https://doi.org/10.2196/15752.
9. Ochalek, T.A., Cumpston, K.L., Wills, B.K., Gal, T.S., and Moeller, F.G. (2020). Nonfatal Opioid Overdoses at an Urban Emergency Department During the COVID-19 Pandemic. JAMA *324*, 1673–1674. https://doi.org/10.1001/JAMA.2020.17477.
10. Slavova, S., Rock, P., Bush, H.M., Quesinberry, D., and Walsh, S.L. (2020). Signal of increased opioid overdose during COVID-19 from emergency medical services data. Drug Alcohol Depend. *214*, 108176. https://doi.org/10.1016/J.DRUGALCDEP.2020.108176.
11. National Institute on Drug Abuse. Drug Overdose Death Rates. https://nida.nih.gov/research-topics/trends-statistics/overdose-death-rates.
12. Dhowan, B., Lim, J., MacLean, M.D., Berman, A.G., Kim, M.K., Yang, Q., Linnes, J., Lee, C.H., Goergen, C.J., and Lee, H. (2019). Simple minimally-invasive automatic antidote delivery device (A2D2) towards closed-loop reversal of opioid overdose. J. Contr. Release *306*, 130–137. https://doi.org/10.1016/j.jconrel.2019.05.041.
13. Imtiaz, M.S., Bandoian, C.V., and Santoro, T.J. (2021). Hypoxia driven opioid targeted automated device for overdose rescue. Sci. Rep. *11*, 24513. https://doi.org/10.1038/s41598-021-04094-x.
14. Lombardi, A.R., Arya, R., Rosen, J.G., Thompson, E., Welwean, R., Tardif, J., Rich, J.D., and Park, J.N. (2023). Overdose Detection Technologies to Reduce Solitary Overdose Deaths: A Literature Review. Int. J. Environ. Res. Publ. Health *20*, 1230. https://doi.org/10.3390/IJERPH20021230.
15. Mahmud, M.S., Fang, H., Wang, H., Carreiro, S., and Boyer, E. (2018). Automatic Detection of Opioid Intake Using Wearable Biosensor. In 2018 International Conference on Computing, Networking and Communications (ICNC) (Institute of Electrical and Electronics Engineers Inc.), pp. 784–788. https://doi.org/10.1109/ICCNC.2018.8390334.
16. Nandakumar, R., Gollakota, S., and Sunshine, J.E. (2019). Opioid overdose detection using smartphones. Sci. Transl. Med. *11*, eaau8914.
17. Kanter, K., Gallagher, R., Eweje, F., Lee, A., Gordon, D., Landy, S., Gasior, J., Soto-Calderon, H., Cronholm, P.F., Cocchiaro, B., et al. (2021). Willingness to use a wearable device capable of detecting and reversing overdose among people who use opioids in Philadelphia. Harm Reduct. J. *18*, 75. https://doi.org/10.1186/s12954-021-00522-3.
18. Lombardi, A.R., Arya, R., Rosen, J.G., Thompson, E., Welwean, R., Tardif, J., Rich, J.D., and Park, J.N. (2023). Overdose Detection Technologies to Reduce Solitary Overdose Deaths: A Literature Review. Int. J. Environ. Res. Publ. Health *20*, 1230. https://doi.org/10.3390/IJERPH20021230.
19. Schreyer, K.E., Malik, S., Blome, A., and D'Orazio, J.L. (2020). A Case Report of a Novel Harm Reduction Intervention Used to Detect Opioid Overdose in the Emergency Department. Clin. Pract. Cases Emerg. Med. *4*, 548–550. https://doi.org/10.5811/CPCEM.2020.7.47936.
20. Kooij, L., Peters, G.M., Doggen, C.J.M., and van Harten, W.H. (2022). Remote continuous monitoring with wireless wearable sensors in clinical practice, nurses perspectives on factors affecting implementation: a qualitative study. BMC Nurs. *21*, 53. https://doi.org/10.1186/S12912-022-00832-2.

21. Mekhael, M., Ho, C., Noujaim, C., Assaf, A., Younes, H., El Hajjar, A.H., Chaudhry, H.A., Lanier, B., Chouman, N., Makan, N., et al. (2023). Compliance Challenges in a Longitudinal COVID-19 Cohort Using Wearables for Continuous Monitoring: Observational Study. J. Med. Internet Res. *25*, e43134. https://doi.org/10.2196/43134.

22. Stuart, T., Hanna, J., and Gutruf, P. (2022). Wearable devices for continuous monitoring of biosignals: Challenges and opportunities. APL Bioeng. *6*, 021502. https://doi.org/10.1063/5.0086935.

23. Chan, J., Iyer, V., Wang, A., Lyness, A., Kooner, P., Sunshine, J., and Gollakota, S. (2021). Closed-loop wearable naloxone injector system. Sci. Rep. *11*, 22663. https://doi.org/10.1038/s41598-021-01990-0.

24. Ahamad, K., Dong, H., Johnson, C., Hyashi, K., DeBeck, K., Milloy, M.J., and Wood, E. (2019). Factors associated with willingness to wear an electronic overdose detection device. Addiction Sci. Clin. Pract. *14*, 23. https://doi.org/10.1186/s13722-019-0153-5.

25. Darke, S., Larney, S., and Farrell, M. (2017). Yes, people can die from opiate withdrawal. Addiction *112*, 199–200. https://doi.org/10.1111/ADD.13512.

26. FDA. FDA Approves Higher Dosage of Naloxone Nasal Spray to Treat Opioid Overdose. https://www.fda.gov/news-events/press-announcements/fda-approves-higher-dosage-naloxone-nasal-spray-treat-opioid-overdose.

27. Moss, R.B., Pryor, M.M., Baillie, R., Kudrycki, K., Friedrich, C., Reed, M., and Carlo, D.J. (2020). Higher naloxone dosing in a quantitative systems pharmacology model that predicts naloxone-fentanyl competition at the opioid mu receptor level. PLoS One *15*, e0234683. https://doi.org/10.1371/JOURNAL.PONE.0234683.

28. Rzasa Lynn, R., and Galinkin, J.L. (2018). Naloxone dosage for opioid reversal: current evidence and clinical implications. Ther. Adv. Drug Saf. *9*, 63–88. https://doi.org/10.1177/2042098617744161.

29. Bisignani, A., De Bonis, S., Mancuso, L., Ceravolo, G., and Bisignani, G. (2019). Implantable loop recorder in clinical practice. J. Arrhythm. *35*, 25–32. https://doi.org/10.1002/joa3.12142.

30. Lelovas, P.P., Kostomitsopoulos, N.G., and Xanthos, T.T. (2014). A Comparative Anatomic and Physiologic Overview of the Porcine Heart. J. Am. Assoc. Lab. Anim. Sci. *53*, 432–438.

31. Walters, E.M., and Prather, R.S. (2013). Advancing Swine Models for Human Health and Diseases. Mo. Med. *110*, 212–215.

32. Bernardini, A., Brunello, A., Gigli, G.L., Montanari, A., and Saccomanno, N. (2022). OSASUD: A dataset of stroke unit recordings for the detection of Obstructive Sleep Apnea Syndrome. Sci. Data *9*, 177. https://doi.org/10.1038/s41597-022-01272-y.

33. Zwillich, C., Devlin, T., White, D., Douglas, N., Weil, J., and Martin, R. (1982). Bradycardia during sleep apnea. Characteristics and mechanism. J. Clin. Invest. *69*, 1286–1292. https://doi.org/10.1172/JCI110568.

34. Liu, G.Z., Guo, Y.W., Zhu, Q.S., Huang, B.Y., and Wang, L. (2011). Estimation of Respiration Rate from Three-Dimensional Acceleration Data Based on Body Sensor Network. Telemed. J. E. Health. *17*, 705–711. https://doi.org/10.1089/TMJ.2011.0022.

35. Elgendi, M. (2012). On the Analysis of Fingertip Photoplethysmogram Signals. Curr. Cardiol. Rev. *8*, 14–25. https://doi.org/10.2174/157340312801215782.

36. Dowell, D., Ragan, K.R., Jones, C.M., Baldwin, G.T., and Chou, R. (2022). CDC Clinical Practice Guideline for Prescribing Opioids for Pain — United States, 2022. MMWR Recomm. Rep. *71*, 1–95. https://doi.org/10.15585/MMWR.RR7103A1.

37. Kohler, A., Blendinger, F., Müller, S., Mescheder, U., and Bucher, V. (2023). Feasibility of Parylene C for encapsulating piezoelectric actuators in active medical implants. Front. Med. Technol. *5*, 1211423. https://doi.org/10.3389/FMEDT.2023.1211423.

38. Chong, H., Majerus, S.J.A., Bogie, K.M., and Zorman, C.A. (2020). Nonhermetic packaging of biomedical microsystems from a materials perspective: A review. Med. Devices Sens. *3*, e10082. https://doi.org/10.1002/MDS3.10082.

39. Sang, M., Kim, K., Shin, J., and Yu, K.J. (2022). Ultra-Thin Flexible Encapsulating Materials for Soft Bio-Integrated Electronics. Adv. Sci. *9*, 2202980. https://doi.org/10.1002/ADVS.202202980.

40. Huang, H.W., Khandelwal, N., Kerssemakers, T., Ballinger, I., and Traverso, G. (2023). Power optimization in Battery-Powered Micro-Motors. In 2022 IEEE International Conference on Cyborg and Bionic Systems (CBS) (IEEE), pp. 274–279. https://doi.org/10.1109/CBS55922.2023.10115384.

41. Leary, S., Underwood, W., Anthony, R., Cartner, S., Grandin, T., Greenacre, C., Gwaltney-Brant, S., McCrackin, M.A., Meyer, R., Miller, D., et al. (2020). AVMA Guidelines for the Euthanasia of Animals: 2020 edition (American Veterinary Medical Association).